Journal of Cleaner Production 544 (2026) 147718

Contents lists available at ScienceDirect

Journal of Cleaner Production

journal homepage: www.elsevier.com/locate/jclepro

Improving the performance of recycled EN 45500: a sustainable approach through heat treatment optimization

Cristian Cascioli *, Linda Castagnini, Alessandro Morri, Lorella Ceschini

Department of Industrial Engineering, Alma Mater Studiorum - University of Bologna, Italy

GRAPHICAL ABSTRACT

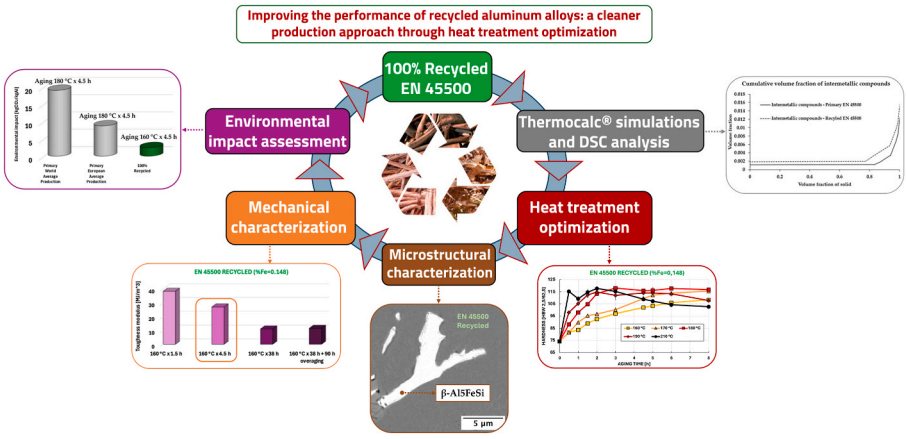

ARTICLE INFO

Keywords:
Aluminum
EN 45500
AlSi7Cu0.5Mg0.3
Recycling
Aging optimization
Sustainability

ABSTRACT

This study investigates the performance and environmental impact of a 100% recycled EN 45500 aluminum alloy subjected to T6 heat treatment, using its primary counterpart as a benchmark. Both alloys were produced by gravity die casting under controlled laboratory conditions and subsequently characterized from a microstructural and mechanical standpoint. The recycled alloy exhibited a higher iron content, promoting the formation of Fe-based intermetallic compounds, which increased defect density and reduced ductility compared to the primary alloy. Heat treatment parameters were optimized to balance mechanical performance with energy efficiency. Tensile testing revealed that the recycled alloy achieved mechanical properties comparable to those of the peak-aged primary alloy when aged at 160 °C for 4.5 h, a less energy-intensive condition than the 180 °C for 4.5 h required by the primary alloy. The environmental impact analysis demonstrated a significant reduction in carbon footprint, from 19.6 $kgCO_{2eq}$/kgAl for the primary alloy to 2.47 $kgCO_{2eq}$/kgAl for the recycled one. For 100% recycled EN 45500 alloy, the heat treatment, including solution treatment and aging, accounted for 92.3% of CO_{2eq} emissions, underscoring the relevance of heat treatment optimization. Overaging tests demonstrated that the recycled EN 45500 retained copper-driven thermal stability. Overall, the findings highlight the capability of

* Corresponding author. Viale del Risorgimento 4, Bologna, Italy.
E-mail addresses: cristian.cascioli2@unibo.it (C. Cascioli), linda.castagnini2@unibo.it (L. Castagnini), alessandro.morri4@unibo.it (A. Morri), lorella.ceschini@unibo.it (L. Ceschini).

https://doi.org/10.1016/j.jclepro.2026.147718
Received 5 December 2025; Received in revised form 23 January 2026; Accepted 1 February 2026

recycled aluminum to meet both mechanical performance and sustainability requirements to produce advanced automotive applications.

1. Introduction

Aluminum is the most widely produced non-ferrous metal globally, with extensive applications in several sectors, including energy, aerospace, and automotive. Its alloys are highly valued in the transport industry for their advantageous combination of properties, including a high strength-to-weight ratio, good corrosion resistance, elevated thermal and electrical conductivity, and excellent processability (Li et al., 2023). Among casting techniques, gravity die casting remains dominant for automotive components, offering energy efficiency and design flexibility (Ducker, 2023). Within this context, Al–Si–Mg alloys, typically containing limited copper additions (0.5–1.5 wt%), are widely used in powertrain components such as engine blocks and cylinder heads, and their use is also expanding in electric vehicles (EVs) (Rolseth et al., 2024).

The hypoeutectic EN 45500 alloy (AlSi7Cu0.5Mg0.3), obtained from EN 42100 through the addition of approximately 0.5 wt% Cu, retains the excellent castability and mechanical performance of EN 42100 ((Di Sabatino et al., 2005), (Ceschini et al., 2011)), while the copper addition imparts enhanced thermal stability, making the alloy particularly suitable for modern engine components. This is especially relevant in current powertrain design, where engine downsizing, higher combustion pressures, and increased thermal loads impose more severe operating conditions and require materials capable of maintaining strength, and dimensional stability at elevated temperatures (Ceschini et al., 2016).

Despite these advantages, the environmental impact of aluminum alloy production must be considered. Primary aluminum production is highly energy-intensive, largely due to the Hall–Héroult electrolytic reduction process, which typically relies on fossil fuel-based electricity. This process alone accounts for approximately 1% of global anthropogenic greenhouse gas emissions and consumes nearly 1% of the world's total electricity (~13 EJ per year) (Raabe et al., 2022). Consequently, recycled aluminum alloys are increasingly attractive for the automotive industry, as remelting scrap requires only about 2.8 kWh/kg, compared with approximately 45 kWh/kg for primary production (Raabe et al., 2022). This corresponds to an energy saving of over 90% and to a CO_{2eq} emission reduction of about 95%, strongly supporting global decarbonization and emission-reduction policies.

However, each remelting cycle increases iron (Fe) content in recycled alloys (Cagala et al., 2013). High Fe content promotes the formation of Fe-rich intermetallic compounds, generally regarded as detrimental to alloy performance because they promote interdendritic shrinkage and reduce ductility and fatigue resistance ((Ceschini et al., 2009), (Taylor, 2004)). Targeted mitigation strategies, such as sedimentation, can reduce Fe content but are energy-intensive and generate residual waste ((Harazeen et al., 2025), (Nunes et al., 2023)). Since no industrially feasible solution has yet been widely implemented, a comprehensive understanding of the effects of Fe-based intermetallics on mechanical properties is crucial to fully assess the potential of recycled aluminum alloys for automotive applications.

Compositional differences between primary and recycled alloys also affect the response to heat treatment. The T6 treatment, comprising solution treatment, quenching, and artificial aging, is commonly employed to enhance strength and hardness. While optimal T6 parameters are well established for primary EN 45500 alloys ((Ibrahim et al., 2016), (Samuel, 2012)), variations in chemical composition and microstructure in recycled alloys may reduce treatment efficiency, requiring tailored heat treatment cycles. Furthermore, conventional high-temperature aging is energy-intensive and can accelerate precipitation, often at the expense of mechanical performance. Conversely, lower-temperature aging could offer a promising trade-off between mechanical optimization and energy efficiency.

Although the role of copper in improving high-temperature performance is well known, limited attention has been devoted to its recycling and retention in recycled aluminum alloys. Achieving circularity requires not only the recovery of the aluminum matrix but also of critical alloying elements such as Cu (Koese et al., 2025). In the European Union (EU), over 60% of Cu demand relies on imports, with secondary sources contributing only about 40% of total consumption. Despite the high recyclability of Cu, end-of-life recycling rates remain near 60%, due to material dissipation, non-functional recycling, and scrap exports (Ciacci et al., 2020). Systematic studies addressing how recycling-induced compositional variability affects Cu-containing phases in Al–Si–Cu–Mg alloys are still limited, constraining their broader industrial adoption.

In this context, the present study aims to characterize a commercially available primary and a 100% recycled EN 45500 alloys currently used in industrial practice, through a direct comparison focusing on their heat treatment response, mechanical properties, and microstructural features. A laboratory-scale assessment of environmental impact is also presented, comparing an optimized T6 treatment for the primary alloy with an energy-efficient cycle yielding equivalent mechanical performance in the recycled alloy. Finally, the influence of recycling-derived contaminant elements on the overaging behaviour of the EN 45500 alloy is analysed, providing insights for sustainable process optimization.

2. Materials and methods

2.1. Analysed materials and casting process

Two EN 45500 alloys were investigated: a reference alloy produced from primary aluminum (Galf S.r.l.), and a fully recycled alloy produced from industrial post-consumer aluminum scrap supplied by Raffmetal S.p.A. According to the supplier's Environmental Product Declaration (EPD) (Raffmetal, 2023), the recycled aluminum ingots were obtained through a controlled industrial recycling route, including scrap collection from European sources, followed by sorting and pre-treatment operations aimed at separating aluminum from non-metallic materials and other metals. Scrap pre-treatment involved mechanical processing (size reduction and compaction) and decoating, designed to minimize surface contaminants prior to remelting. The scrap remelting stage was carried out using protective saline fluxes (NaCl–KCl mixtures) to limit oxidation and to promote the removal of impurities. The alloys were than processed on a laboratory scale using an 8-kW vacuum-assisted induction die casting machine (TVC10S, TOPCAST S.r.l., Arezzo, Italy). Ingots (1 kg) were melted at 750 °C under a protective Ar atmosphere, with the addition of 15 g of AlTi5B1 (~0.075 wt% Ti) and 0.8 g of AlSr10 master alloy grain refinement and eutectic silicon modification, respectively. These additions were carefully selected to achieve the Ti content specified by EN 1706:2020 and to optimize the eutectic Si morphology, while maintaining Sr levels within the 100–200 ppm range to avoid porosity issues (Wang et al., 2019). During the laboratory-scale remelting, no additional melt refining treatments were applied to either the primary or recycled alloys. Both the steel mold and charge were preheated to 300 °C to minimize thermal gradients and mitigate solidification-related defects. The molten alloy was immediately poured into the preheated mold under vacuum and Ar protection. After solidification, the casting was extracted and water-quenched at ambient temperature.

The chemical composition of as-cast samples was determined by Glow Discharge Optical Emission Spectroscopy (GD-OES, GDA-650, Spectruma Analytik GmbH, Hof, Bavaria, Germany). The average

values from three measurements are reported in Table 1 and comply with the composition limits specified in EN 1706:2020 (BS EN 1706:2020, 2020).

The recycled alloy contains a relatively high Fe content (0.15 wt%), close to the upper Fe levels commonly recommended for high-performance automotive applications (Cascioli et al., 2025). In this study, no compositional modifications were applied, as the investigated alloy reflects a commercially available material currently used in industrial practice.

Each casting produced two semi-finished cylinders (Fig. 1). Metallographic samples were extracted from the lower sections, while the remaining material was machined into tensile specimens according to ISO 6892-1:2019 (BS EN ISO 6892-1:2019, 2019). For heat treatment optimization, additional samples were collected from the bottom of the risers, as illustrated in Fig. 1.

2.2. Thermodynamic calculations

To analyse the compositional variations induced by recycling on the solidification behaviour of EN 45500 alloys, Scheil simulations with back diffusion in the primary phase were performed using Thermo-Calc® 2025a software with the TCAl9 thermodynamic and MOBAl8 mobility databases. The simulations predict the non-equilibrium solidification sequence of both the primary and recycled alloys using the chemical compositions determined by GD-OES and reported in Table 1. The calculations account for solute microsegregation effects and provide detailed insight into how compositional variations influence the solidification sequence, phase chemistry, and volume fraction of the key phases associated with the main alloying elements (Al, Si, Cu, Mg, Fe, Mn, and Ti).

2.3. Differential Scanning Calorimetry analyses

Differential Scanning Calorimetry (DSC) analyses were performed to investigate the thermal behaviour of the EN 45500 alloy in both its primary and fully recycled (100%) forms, under as-cast (AC) and solution-treated plus quenched (SQ; solution at 535 °C for 4.5 h, followed by water quenching at 60 °C) conditions. The DSC tests performed on the as-cast samples aimed to determine the melting temperatures of the Al_2Cu phase and to assess variations in the endothermic peaks associated with the melting of the eutectic structures and the aluminum matrix. For the SQ samples, the objective was to assess potential differences in the exothermic precipitation mechanisms of coherent, semi-coherent, and incoherent strengthening precipitates, as well as to determine whether any residual Al_2Cu phase was present after a single-step solution treatment.

2.4. Aging and overaging behaviour

A critical analysis of heat treatment parameters is essential to achieve the desired mechanical properties within an industrially feasible timeframe. In this study, specimens underwent T6 heat treatment under varying temperatures and durations, as detailed in Table 2. Solution treatment was performed in a laboratory furnace (LT 9/14, Nabertherm GmbH, Lilienthal, Germany) at 535 °C for 4.5 h. The temperature was continuously monitored using two calibrated thermocouples (accuracy ±1% of the measured value) to ensure uniformity and reproducibility. Immediately after solution treatment, specimens were quenched in water at 60 ± 5 °C, following industrial practice to minimize residual stresses and quench-distortion, particularly in large and complex-shaped castings. Artificial aging was subsequently carried out in the same furnace at six temperatures ranging from 160 to 210 °C, in 10 °C increments. The age-hardening response was evaluated through Brinell hardness measurements (HBW 2.5/62.5) in accordance with ASTM E10 (E28 Committee), using a QATM durometer (QNESS 150 CS, ATM Qness GmbH, Mammelzen, Germany) with a 62.5 kgf load and 2.5 mm tungsten carbide ball. Aging times ranged from 0.5 to 8 h, with 0.5 h increments, consistent with industrial feasibility. At 160 °C, no peak-aging condition was reached within the first 8 h, so the aging duration was extended up to 38 h. For each condition, at least three indentations were performed, and the mean values and standard deviations were reported.

Since Al-Si-Cu-Mg alloys are widely employed in high-temperature automotive applications, such as engine heads, their overaging behaviour was also investigated. Peak-aged specimens were subjected to overaging at 160 °C for further 8, 32, 96, and 128 h to simulate long-term thermal exposure and to assess the evolution of mechanical properties, with particular attention to the potential influence of Fe-rich intermetallics on the Cu-strengthened matrix (Stanić et al., 2020).

2.5. Microstructural analyses

A comprehensive microstructural characterization was performed on both the primary and recycled alloys. Metallographic samples were extracted from the castings, as shown in Fig. 1, and prepared following standard metallographic procedures (E04 Committeea). The samples were mounted in conductive resin, ground with SiC papers up to P2500 grit, and polished using polycrystalline diamond suspensions down to 1 μm. To enhance the contrast between the aluminum matrix and the eutectic constituents, samples were etched with Keller's reagent (95 mL H_2O, 2.5 mL HNO_3, 1.5 mL HCl, 1.0 mL HF) for 10 s at room temperature (E04 Committeeb).

Microstructural observations were conducted using Optical Microscopy (Axioscope 7, Zeiss) and Field Emission Gun Scanning Electron Microscopy (FEG-SEM, Mira3, Tescan), equipped with Energy Dispersive X-ray Spectroscopy (EDS) for phase identification. Quantitative analyses were carried out with ImageJ (v1.54p), focusing on Secondary Dendrite Arm Spacing (SDAS), eutectic silicon morphology, intermetallic phases, and solidification-related defects.

SDAS was measured from optical micrographs (1400 × 800 μm) by analysing at least ten dendrites on three representative images per sample (Ravindran, 2017). The eutectic silicon modification level was assessed from images with a 260 × 150 μm field of view according to the American Foundry Society (AFS) guidelines (Djurdjevic et al., 2001). Intermetallic phases were examined on FEG-SEM micrographs, and their chemical composition was determined via EDS. The area fraction of casting defects was determined from non-etched samples using optical micrographs with a 2800 × 1600 μm field of view (five images per sample). All quantitative data were statistically processed to ensure reproducibility, calculating mean values and standard deviations for each microstructural and mechanical parameter.

2.6. Mechanical characterization

Tensile tests were performed on heat-treated specimens, focusing on

Table 1
Chemical composition (wt.%.) of the primary and recycled EN 45500 alloys obtained by GD-OES.

ALLOY		RECYCLING RATE	Si	Fe	Mn	Mg	Cu	Ti	Sr	Al
EN 45500	PRIMARY	0 %	7.01 ± 0.07	0.07 ± 0.01	0.07 ± 0.02	0.39 ± 0.01	0.54 ± 0.05	0.11 ± 0.01	0.02 ± 0.01	Bal.
	RECYCLED	100 %	6.79 ± 0.04	0.15 ± 0.09	0.03 ± 0.01	0.40 ± 0.02	0.47 ± 0.04	0.15 ± 0.01	0.02 ± 0.01	Bal.
	EN 1706:2020	-	6.5-7.5	0-0.25	0-0.15	0.25-0.45	0.2-0.7	0-0.20	0-0.03	Bal.

Fig. 1. Extraction zones from a EN 45500 casting of samples used for microstructural analyses and mechanical tests.

Table 2
Tested aging parameters.

Solution treatment	Quenching	Artificial aging	
		T [°C]	t [h]
535 °C for 4.5 h	H_2O at 60 °C	160	0.5
		170	1
		180	1.5
		190	2
		200	3
		210	4.5
			5
			6
			8

peak-aged and other industrially relevant conditions (160 - 180 - 210 °C for 1.5 h and 4.5 h). The tests were performed in accordance with ISO 6892-1:2019 (BS EN ISO 6892-1:2019, 2019) using a screw-driven tensile testing machine (Giuliani Italsigma, Forlì, Italy) under displacement control, with a data acquisition frequency of 20 Hz. At least three specimens were tested for each condition, and key tensile properties, including yield strength (YS), ultimate tensile strength (UTS), elongation to failure (e%), and toughness modulus (UT) were evaluated. Additionally, tensile tests were performed on samples tested 90 h after reaching peak hardness in order to mechanically characterize the overaging region from a mechanical point of view (Cascioli et al., 2025).

2.7. Fractographic characterization

High magnification characterization of the fracture surfaces was conducted using FEG-SEM coupled with EDS to investigate failure mechanisms. Secondary electron (SE) imaging was used to characterize the fracture surface morphology and identify fracture mechanisms, with particular attention to the influence of solidification-related defects. Backscattered electron (BSE) imaging provided compositional contrast, enabling the detection of Fe- and Cu-rich intermetallic compounds within the α-Al matrix, whose chemical composition was determined via EDS. Quantitative EDS analyses were performed on at least three fields of view (520 × 520 μm each) per sample to evaluate the distribution and amount of Fe- and Cu-rich compounds.

2.8. Environmental impact evaluation

This section presents an innovative integration of process-level energy monitoring and life cycle data to evaluate the environmental performance of both the primary and 100% recycled EN 45500 alloy. To complement the mechanical assessment with an environmental impact analysis, the energy consumption of the furnaces during the heat treatment processes was monitored using an electric energy current meter. In addition to the energy consumption during heat treatment, the production-phase carbon footprint of the alloy was included in the assessment. For primary aluminum, global and European average datasets were used (European Aluminium Brussels, 2020), whereas for recycled aluminum, detailed data were provided directly by the producer (Raffmetal, 2025), as reported in Table 3.

The melting phase was not included in the evaluation, as its energy consumption could not be reliably quantified without dedicated metering equipment. Energy data collected in kWh were converted into CO_{2eq} emissions using a country-specific reference emission factor for Italy (1 kWh of electricity generates 0.2563 $kgCO_{2eq}$ according to the ISPRA 2025 report (ISPRA, 2025). This approach ensures consistency with the national energy mix and improves the reliability of the environmental impact estimation.

3. Results and discussion

3.1. Thermodynamic calculations

Non-equilibrium Scheil solidification simulations were performed using Thermo-Calc software for EN 45500 alloys. The evolution of the volume fractions of α-Al, eutectic Si, and intermetallic compounds as a function of the solid fraction is shown in Fig. 2. The simulations revealed a higher cumulative volume fraction of Fe-, Cu-, and Ti-rich intermetallic compounds in the recycled alloy compared with the primary alloy, corresponding to an average increase of 66% (integrated volume

Table 3
Cradle-to-Gate carbon footprint of primary and recycled aluminum alloys productions (European Aluminium Brussels, 2020; Raffmetal, 2025).

Carbon footprint of aluminium alloys productions ($kgCO_{2eq}$/kgAl)		
Primary alloys	Global average	17.0
	European average	6.7
EN 45500 100% Recycled		0.48

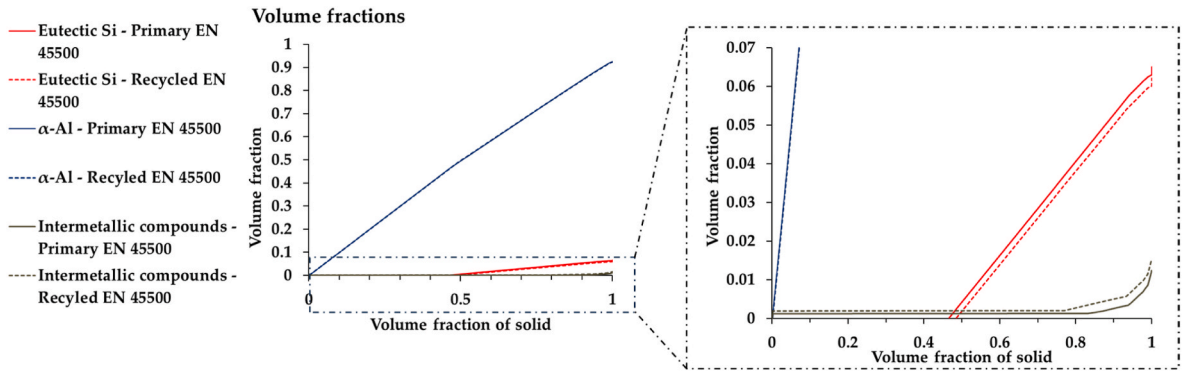

Fig. 2. Non-equilibrium Scheil simulation showing the evolution of the volume fraction of α-Al, eutectic Si, and the cumulative of intermetallic compounds during solidification for the primary (solid line) and recycled (dashed line) EN 45500 alloys.

fraction: primary = 0.0016; recycled = 0.0027). This higher intermetallic content in the recycled alloy was balanced in the primary alloy by a negligible rise in α-Al and by a more substantial increase in eutectic Si. Specifically, the eutectic Si volume fraction increased by 0.0013 in the primary alloy, a value comparable to the variation in total intermetallic phases (0.0011).

The reduced eutectic Si fraction predicted for the recycled alloy can be attributed to the lower Si content, as confirmed by GD-OES analysis (average difference = 0.22 wt%) between the primary and recycled alloys (Table 1).

Focusing on the volume fraction of intermetallic compounds, the simulation (Fig. 3) revealed a markedly higher fraction of β-Al_5FeSi in the recycled alloy, approximately 5.5 times greater than in the primary alloy. This enrichment is consistent with the lower Mn/Fe ratio (0.2), which favours β-phase stabilization. Conversely, in the primary alloy, the higher Mn content (Mn/Fe = 1), promoted the transformation of the β-phase into the more compact α-$Al_{15}(Fe,Mn)_3Si_2$ phase, which showed a 94% higher volume fraction than in the recycled alloy.

The Al_3Ti phase displayed a 61% higher volume fraction in the recycled alloy, consistent with its higher Ti content (0.145 ± 0.001 wt

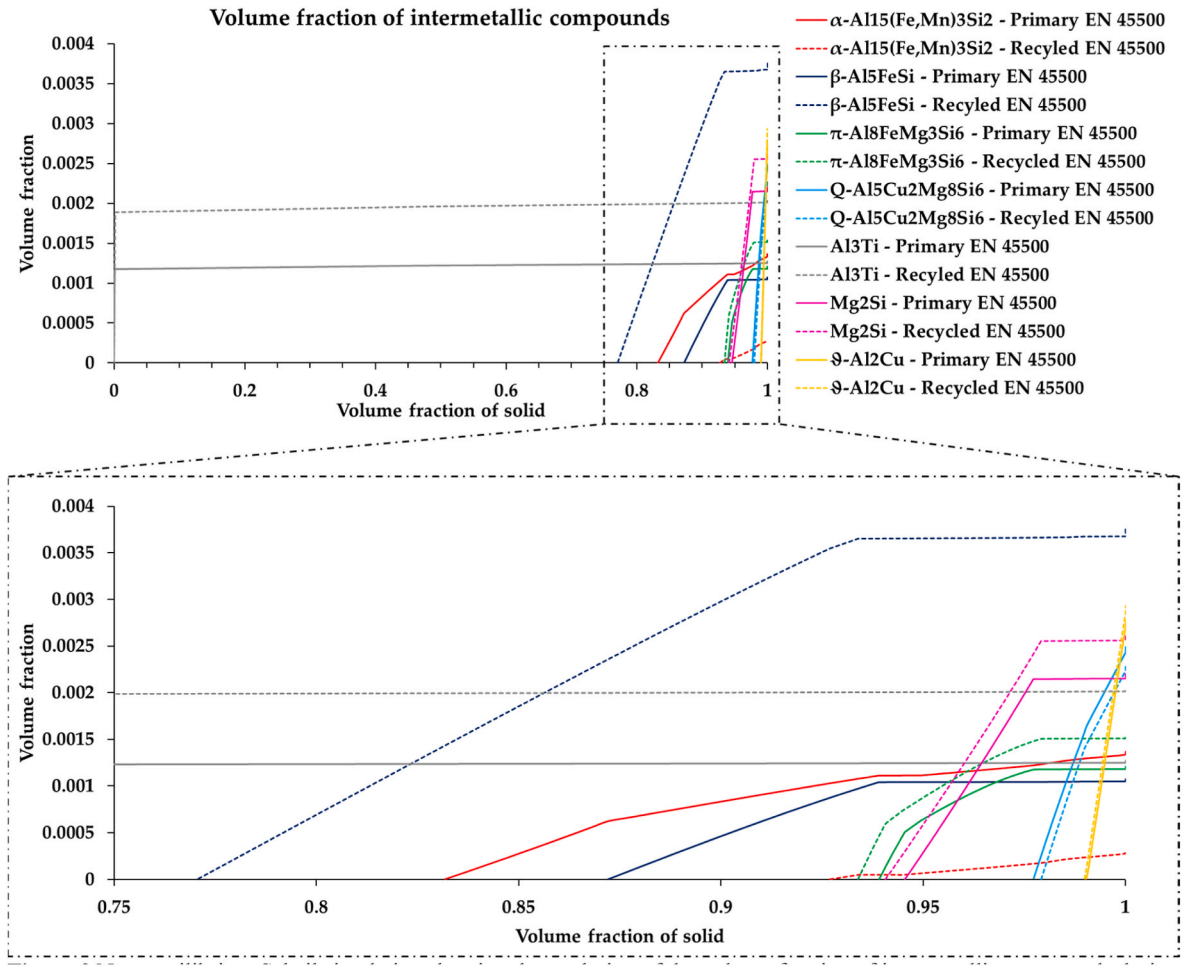

Fig. 3. Non-equilibrium Scheil simulation showing the evolution of the volume fraction of intermetallic compounds during solidification for the primary (solid line) and recycled (dashed line) EN 45500 alloys.

%) compared with the primary alloy (0.110 ± 0.001 wt%) that promoted the solidification of coarse intermetallic compounds.

The π-$Al_8FeMg_3Si_6$ and Mg_2Si phases were predicted to form in comparable volume fractions in both alloys, though slightly higher in the recycled EN 45500 alloy (+34% and +23%, respectively). Finally, the Scheil simulations indicated that both θ-Al_2Cu and Q-$Al_5Cu_2Mg_8Si_6$ formed in limited and comparable volume fractions in the two alloys, consistent with the copper content (~0.5 wt%). This result aligns with recent findings by Li et al. (2025), who reported that a Cu enrichment of the liquid phase (~1.5 wt%) is required to enhance the Cu concentration at the solid-liquid interface and promote the nucleation and growth of Cu-rich intermetallic compounds.

3.2. Differential Scanning Calorimetry analyses

Fig. 4 shows the DSC heating curves of the primary and 100% recycled EN 45500 alloys in the as-cast condition.

Both alloys exhibit comparable thermal profiles, indicating similar phase transformation, although subtle variations can be observed in the intensity and position of the characteristic peaks. Peak B corresponds to the endothermic event related to the melting of the Al_2Cu phase, while peak C represents the main endothermic reaction related to the melting of the eutectic Al–Si. The lower intensity of this peak observed in the recycled alloy can be attributed to its lower Si content, as evidenced by the GD-OES analysis, which limits the formation of eutectic Si, consistent with the Scheil simulation results.

Finally, peak D is associated with the complete melting of the primary α-Al dendritic regions. Overall, the close correspondence between the two curves indicates that recycling does not significantly alter the melting behaviour of the EN 45500 alloy, although minor shifts in peak position highlight subtle microstructural and compositional differences induced by the recycling process.

Fig. 5 presents the DSC heating curves of the primary and 100% recycled EN 45500 alloys after solution treatment at 535 °C for 4.5 h followed by water quenching at 60 °C.

Compared with the as-cast condition, the thermal profiles reveal multiple exothermic peaks at lower temperatures, reflecting the microstructural evolution induced by the heat treatment. The sequence of exothermic events (peaks A1–A3) between 170 °C and 330 °C can be associated with the precipitation of strengthening phases. Specifically, peak A1 corresponds to the formation of coherent θ″ precipitates, peak A2 to the semi-coherent θ′ phase, and peak A3 to incoherent θ (Al_2Cu) particles. At higher temperatures, the endothermic peaks C and D again correspond to the melting of eutectic Al–Cu–Si constituents and the complete melting of the α-Al matrix, respectively. The absence of an endothermic signal in the 555–565 °C range for both alloys confirms that a single-step solution treatment at 535 °C is sufficient to achieve full dissolution of the Al_2Cu phase. Table 4 reports the onset and peak temperatures associated with the exothermic and endothermic events detected in both alloys under the two investigated conditions.

Overall, the DSC analysis confirms that the melting and precipitating behaviour of the recycled EN 45500 alloy remain largely comparable to that of the primary material, although slight shifts in melting events reflect compositional differences associated with the recycling process.

3.3. Aging and overaging behaviour

Fig. 6 shows the 3D surface plots of Brinell hardness HBW [2.5/62.5] as a function of aging temperature and time for the primary (**a**) and recycled (**b**) EN 45500 alloys.

For all the analysed aging conditions, both alloys exhibit the typical precipitation-hardening behaviours of Al–Si–Cu–Mg systems. The formation of β-Mg_2Si and θ-Al_2Cu precursors as coherent and semi-coherent strengthening particles leads to the observed hardness peak (Toschi, 2018). Beyond this point, hardness progressively decreases, particularly at 190 °C, 200 °C, and 210 °C, due to the coarsening of nanoscale precipitates, undetectable via FEG-SEM, marking the onset of overaging (Toschi, 2018).

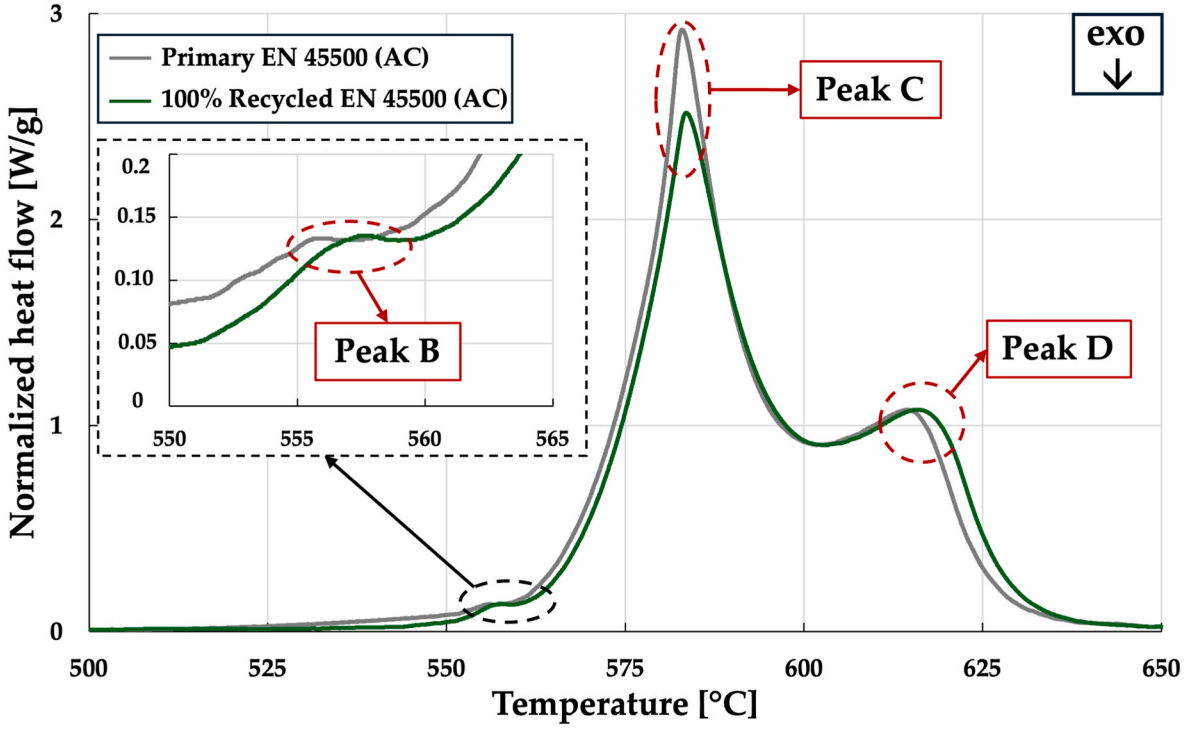

Fig. 4. DSC thermograms of the primary and 100% recycled EN 45500 alloys in the as-cast condition. Both alloys exhibit comparable thermal profiles, indicating similar melting reactions. Peak B corresponds to the endothermic melting of the Al_2Cu phase, while Peak C represents the major endothermic melting of the Al–Si eutectic. The lower intensity of Peak C in the recycled alloy was attributed to its reduced Si content. Finally, Peak D is associated with the complete melting of the primary α-Al dendritic regions.

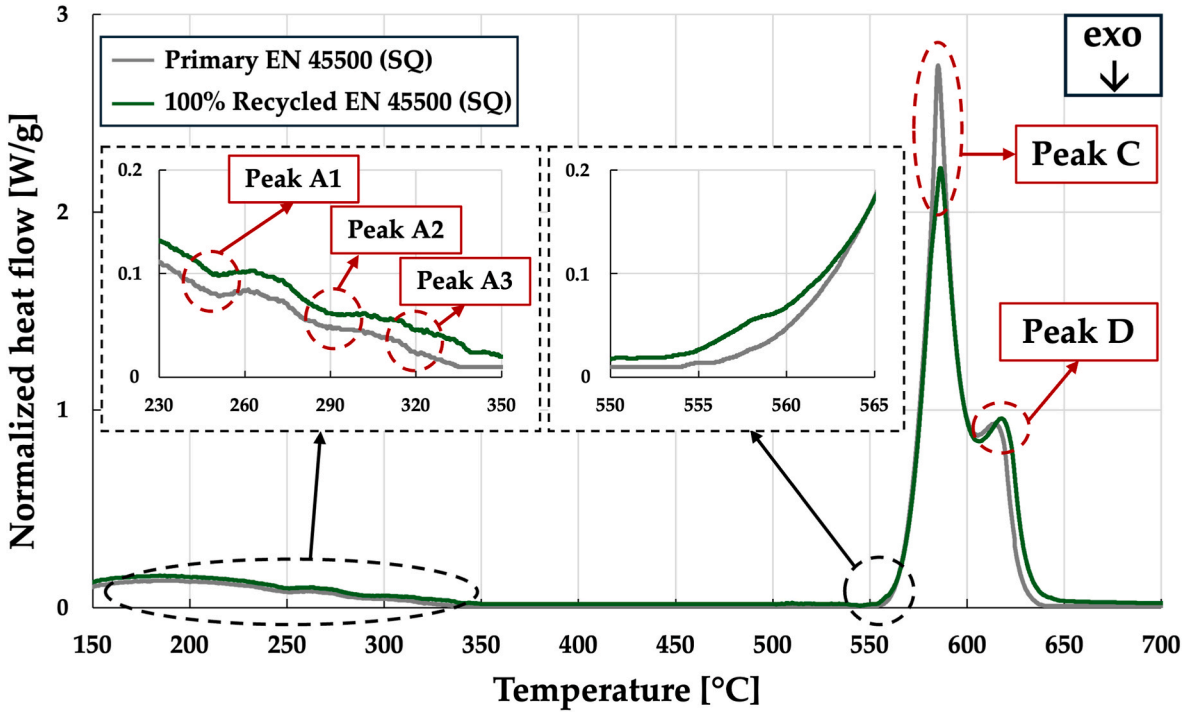

Fig. 5. DSC thermograms of the primary and 100% recycled EN 45500 alloys in the solution-treated and quenched condition. Peak A1 corresponds to the formation of coherent θ″ precipitates, Peak A2 to semi-coherent θ′, and Peak A3 to incoherent θ (Al_2Cu) particles. The absence of a distinct endothermic signal around 555–565 °C in both alloys confirms that the single-step solution treatment at 535 °C effectively dissolves Al_2Cu phases.

Table 4
Summary of magnitudes and temperature ranges of the exothermic and endothermic events for both alloys under the AC and SQ conditions.

			PEAK A1	PEAK A2	PEAK A3	PEAK B	PEAK C	PEAK D
AC	EN 45500 Primary	T_{ONSET}	-	-	-	553.8 °C	557.6 °C	601.9 °C
		T_{PEAK}	-	-	-	554.9 °C	582.9 °C	614.3 °C
	EN 45500 Recycled	T_{ONSET}	-	-	-	554.9 °C	559.0 °C	602.7 °C
		T_{PEAK}	-	-	-	557.9 °C	583.5 °C	616.2 °C
SQ	EN 45500 Primary	T_{ONSET}	172.8 °C	265.0 °C	298.2 °C	-	554.1 °C	605.9 °C
		T_{PEAK}	250.6 °C	289.1 °C	321.0 °C	-	585.1 °C	613.9 °C
	EN 45500 Recycled	T_{ONSET}	175.8 °C	270.5 °C	294.5 °C	-	550.0 °C	605.4 °C
		T_{PEAK}	251.3 °C	293.4 °C	323.1 °C	-	582.4 °C	618.1 °C

As summarized in Table 5, the hardness peak is reached more rapidly at higher temperatures: for example, at 210 °C maximum hardness is attained after just 1.5 h, whereas at 180 °C it occurs after 4.5 h. At 160 °C, no hardness peak was reached within the first 8 h of aging. Aging was therefore extended, and the hardness peak was observed and subsequently exceeded after 38 h, yielding hardness values of 117 ± 0.75 HBW [2.5/62.5] for the primary alloy and 122 ± 0.47 HBW [2.5/62.5] for the recycled alloy.

Overall, the recycled alloy exhibits a hardness evolution comparable to that of the primary alloy, but with slightly higher hardness values. This behaviour can be attributed to the larger amount of Fe-rich intermetallic compounds. Since the Brinell indentation encompasses both the α-Al matrix and the intermetallic phases, the increased fraction of these harder Fe-bearing compounds results in a higher overall measured hardness, despite the reduced content of solute elements available to form strengthening precipitates.

Overaging tests were performed at 160 °C to evaluate the contribution of Cu to the thermal stability of the analysed alloys. This temperature is representative of the operating conditions typically experienced by cylinder heads in standard passenger cars. Fig. 7 compares the overaging behaviour of primary and recycled EN 45500 alloys both aged at 160 °C, expressed as Brinell hardness (HBW [2.5/62.5]) over a period extending up to 144 h beyond the condition of aging at 160 °C for 4.5 h.

Both alloys exhibit a slow and comparable decrease in hardness, highlighted by the linear interpolation of the overaging curves, which present similar negative slopes.

3.4. Microstructural analyses

The microstructural characterization of the heat-treated primary and recycled EN 45500 alloys revealed comparable features across all aging conditions. Representative low magnification optical micrographs of the heat-treated primary and recycled EN 45500 alloys aged at 160 °C for 4.5 h are shown in Fig. 8(a) and (b), respectively. Both alloys exhibit a typical hypoeutectic Al–Si morphology, consisting of a primary dendritic α-Al matrix surrounded by the eutectic (α-Al - Si) constituent.

The SDAS values were comparable for the two alloys, averaging 19 ± 1 μm, in agreement with reported values for laboratory-scale gravity die castings produced at a cooling rate of 9.3 K/s (Li et al., 2020). The eutectic silicon of both alloys exhibited a fibrous morphology corresponding to modification level 5 according to the AFS standard (Djurdjevic et al., 2001), as shown by Fig. 8(c) and (d). The recycled alloy exhibited nearly twice the defect content measured in the primary alloy (2.45 ± 0.53% vs. 1.42 ± 0.28% respectively), as measured on the metallographic samples. These porosity levels are consistent with values reported in the literature for AlSi7Mg alloys produced by gravity die

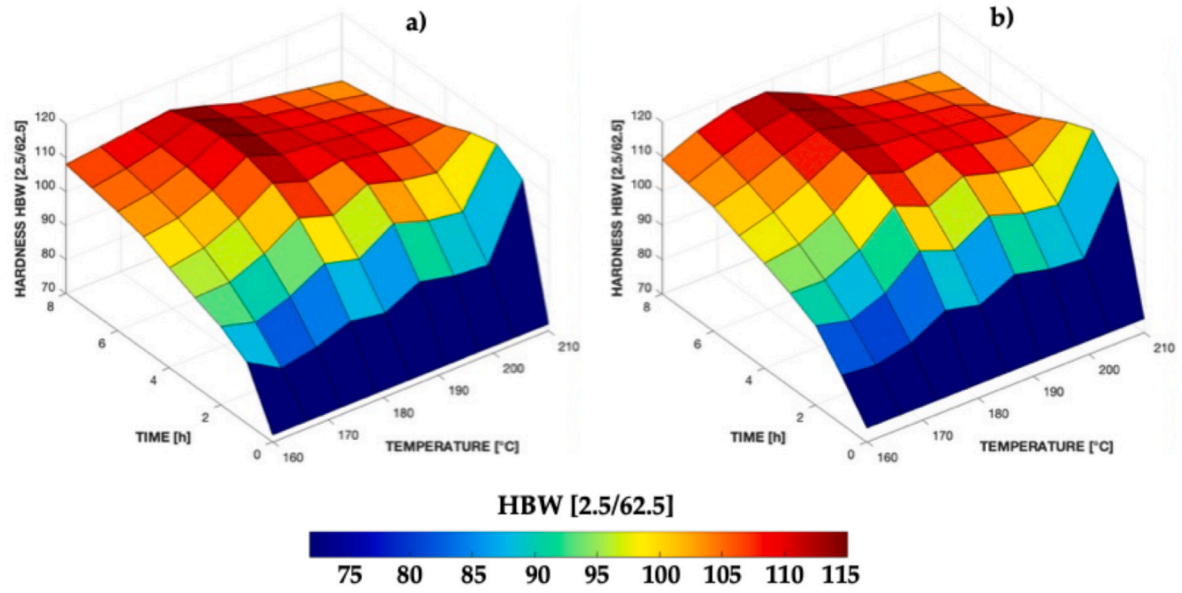

Fig. 6. 3D surface plots of Brinell hardness HBW [2.5/62.5] as a function of aging temperature and time for the primary (**a**) and recycled (**b**) EN 45500 alloys. Both alloys exhibit typical AlSi7Cu0.5Mg0.3 aging behaviour, with peak hardness achieved at shorter times for higher temperatures and slightly higher hardness values for the recycled alloy.

Table 5
Summary of T6 peak aging parameters and corresponding Brinell hardness HBW values [2.5/62.5] for primary and recycled EN 45500 alloy.

Solution	Quenching	Peak Aging Parameters		Peak Aging Hardness HBW [2.5/62.5]	
		T [°C]	Time [h]	Primary	Recycled
535 °C for 4.5 h	H_2O at 60 °C	160 °C – peak not detected within 8 h		-	-
		170	6	110 ± 0.97	116 ± 0.73
		180	4.5	117 ± 0.17	118 ± 0.81
		190	4.5	113 ± 2.14	114 ± 0.29
		200	3	114 ± 0.48	116 ± 0.29
		210	1.5	115 ± 1.53	117 ± 1.15

casting (Zyska, 2021).

Representative micrographs showing the spatial association between shrinkage defects and Fe-rich intermetallic compounds in the recycled alloy are reported in Supplementary Fig. 1. These observations support the interpretation that Fe-based intermetallics can locally hinder interdendritic feeding during solidification, thereby promoting shrinkage defect formation. This interpretation is consistent with the mechanisms described by Taylor (2004), who reported that Fe-rich intermetallic phases, particularly β-Al_5FeSi platelets, can impede interdendritic feeding and increase shrinkage porosity formation in Al–Si casting alloys.

EDS analyses performed on heat-treated specimens were consistent with the simulations of the as-cast alloys. In the primary alloy (Fig. 9(a)), the predominant intermetallic phases were π-$Al_8FeMg_3Si_6$ and α-$Al_{15}(Fe,Mn)_3Si_2$ (with minor Cu traces), whereas in the recycled alloy π-$Al_8FeMg_3Si_6$ and β-Al_5FeSi were dominant (Fig. 9(b)). Among these,

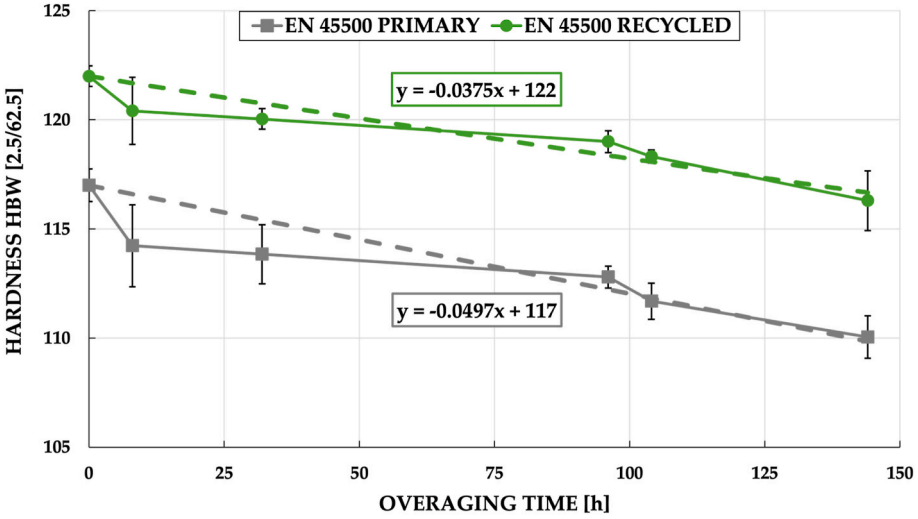

Fig. 7. Overaging behaviours of primary and recycled EN 45500 alloys at 160 °C, expressed as Brinell hardness HBW [2.5/62.5] versus overaging time up to 144 h. Both alloys exhibit a gradual and comparable hardness decrease, highlighting that a high recycled content can still preserve the copper-driven resistance to overaging.

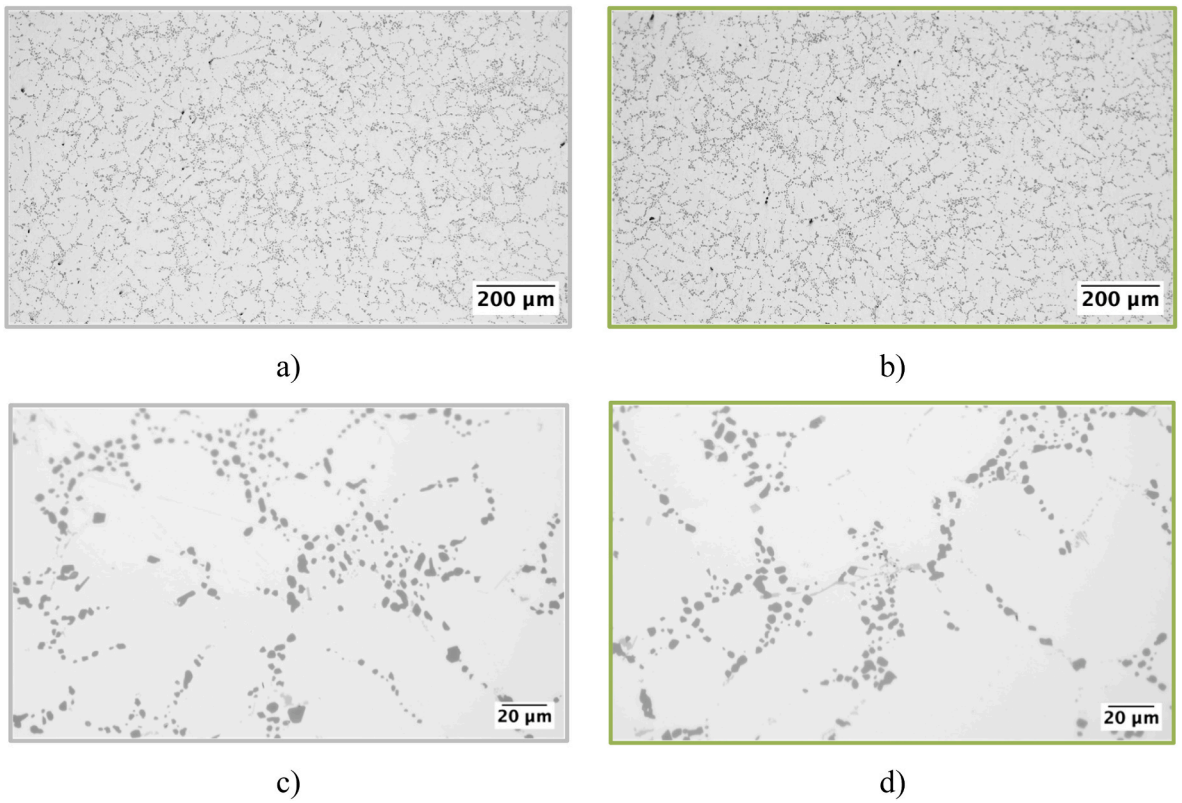

Fig. 8. Representative optical micrographs of the primary (**a,c**) and recycled (**b,d**) EN 45500 alloys in the T6 condition. The recycled alloy exhibits a higher percentage of defects, whereas dendritic structures and eutectic particles appear comparable between the two alloys.

the β-Al_5FeSi phase presence is promoted by the Fe/Mn ratio: while the primary alloy exhibits Fe/Mn = 1, the recycled alloy present Fe/Mn = 5, which is associated with the increased prevalence of β-Al_5FeSi intermetallics and the higher defect content observed in the recycled alloy. This phase tends to block the interdendritic feeding channels, promoting porosity formation due to the reduced permeability and localized hydrogen supersaturation in the interdendritic regions (Puncreobutr et al., 2014). Coarse, non-dissolvable $AlTi_3$ were detected in both alloys (Fig. 9(c)–(d)), remaining stable after solution treatment and aging. This behaviour is consistent with previous findings as reported by Perrin et al. (2025). In contrast, θ-Al_2Cu phases were not observed, due to their dissolution during solution treatment, while only limited amounts of the Q-phase ($Al_5Cu_2Mg_8Si_6$) were detected, consistent with the low Cu content (~0.5 wt%).

3.5. Mechanical characterization

Tensile tests were carried out on the primary EN 45500 alloy under selected aging conditions of industrial relevance (160 - 180 - 210 °C for 1.5 h and 160 -180 - 210 °C for 4.5 h). It is worth emphasizing that achieving an optimal balance between elongation to failure and ultimate tensile strength, effectively quantified through the toughness modulus (UT) (Callister and Rethwisch, 2020), is critical for engine components, particularly in cylinder head regions where cyclic stresses may exceed the yield strength (YS) (Chen et al., 2017). Therefore, among all the evaluated conditions, aging at 180 °C for 4.5 h provided the most favourable strength-ductility balance, delivering the highest UTS (362 MPa), a good YS (293 MPa), and an elongation to failure of 8%. In contrast, although higher elongation values were observed at 160 °C and 180 °C for 1.5 h (15% and 11%, respectively) and at 160 °C for 4.5 h (12%), these conditions resulted in lower strength values, as shown in Fig. 10.

As also reported in the literature (Cascioli et al., 2025), the recycled alloys typically exhibit higher UTS and YS, but lower elongation compared with the primary counterparts when subjected to the same aging conditions. Based on this, the present section investigates whether the recycled EN 45500 alloy can achieve mechanical properties comparable to the optimal performance identified for the primary alloy (362 ± 5 MPa UTS, 293 ± 7 MPa YS, 7.5 ± 0.57% e%), obtained through aging at 180 °C for 4.5 h while using less energy-intensive aging treatments and avoiding the reduction in elongation to failure, by applying underaging conditions. To this end, the recycled EN 45500 alloy was tested at 160 °C for 1.5, 4.5, and 38 h (hardness peak), and the results are summarized in Table 6.

Among the tested conditions reported in Table 6, aging at 160 °C for 4.5 h delivered the most favourable strength–ductility balance for the recycled alloy, reaching a UT of 27.06 ± 6.11 MJ/m^3. Although shorter aging (1.5 h) enhanced ductility and prolonged aging (38 h) increased strength, only the 4.5 h condition provided a balanced response that closely approximates the performance of the primary alloy, while operating at a lower temperature and therefore reducing the carbon footprint of the aging process. These findings demonstrate that appropriately tailored thermal treatments can unlock the potential of recycled Al–Si–Cu-Mg alloys, enabling them to meet demanding mechanical performance targets while simultaneously lowering the environmental impact associated with heat treatment. By adjusting the aging conditions, the mechanical response of the recycled EN 45500 alloy can be effectively tuned, allowing different strength to ductility trade-offs to be achieved depending on component requirements, even though the attainable elongation remains lower than that of the primary alloy.

To assess mechanical stability in the overaged regime, further tensile tests were carried out on both alloys after 90 h of additional aging beyond the peak aged condition (160 °C for 38 h), as shown in Fig. 11.

The results confirm that the tensile properties of both the primary and recycled EN 45500 alloys remain essentially unchanged after prolonged thermal exposure. Yield strength, ultimate tensile strength, and

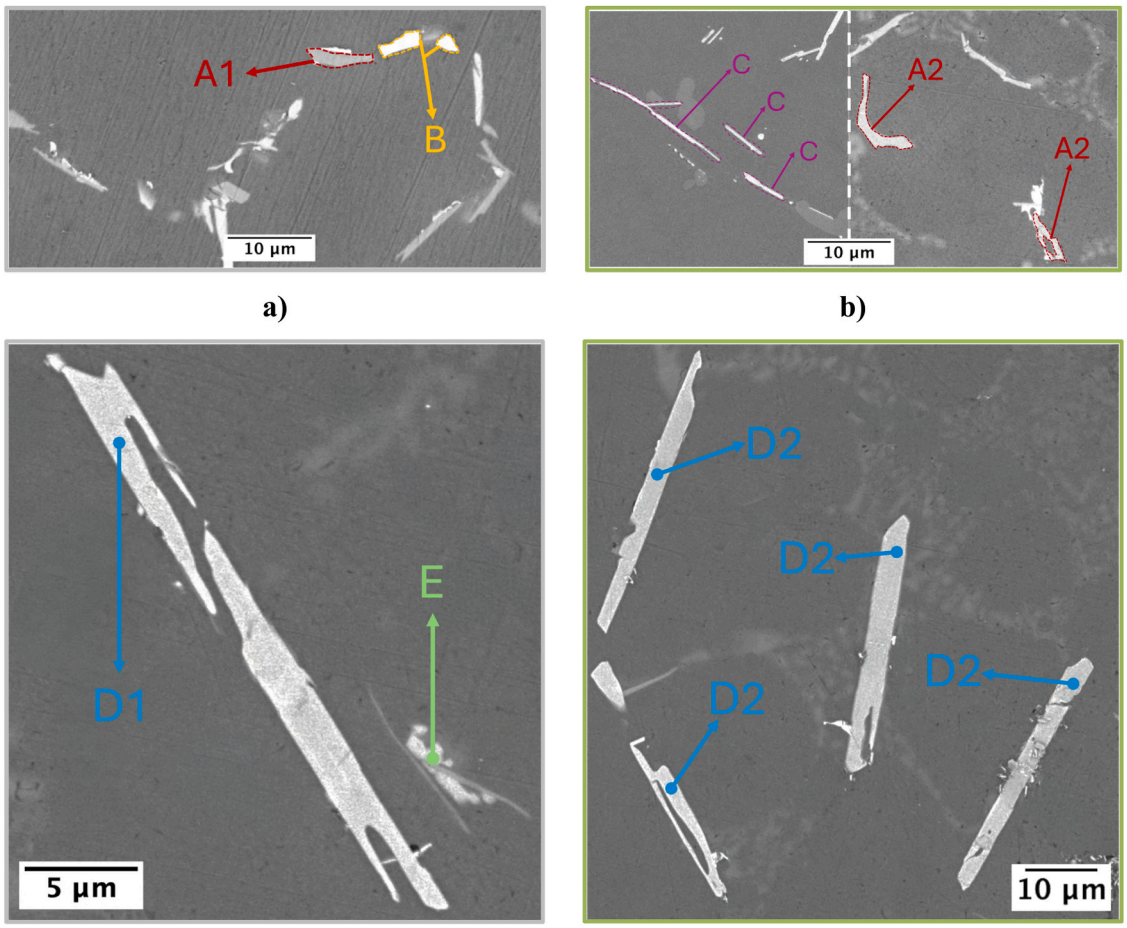

Identified Phase	Spot ID	Al (at.%)	Si (at.%)	Fe (at.%)	Mg (at.%)	Cu (at.%)	Mn (at.%)	Ti (at.%)
π-$Al_8FeMg_3Si_6$	A1	45.3±1.1	33.9±1.0	4.9±0.6	15.9±0.5	-		-
π-$Al_8FeMg_3Si_6$	A2	47.0±1.0	32.3±1.1	5.6±0.7	14.6±0.6	-	-	-
α-$Al_{15}(Fe,Mn,Cu)_3Si_2$	B	61.1±1.2	11.0±0.9	7.9±0.7	-	5.3±0.2	14.7±0.9	-
β-Al_5FeSi	C	55.4±0.7	26.4±0.6	18.2±0.7	-	-	-	-
Al_3Ti	D1	43.6±0.9	11.4±1.2	-	-	-	-	45.0±0.3
Al_3Ti	D2	55.5±0.7	14.2±0.9	-	-	-	-	30.3±1.3
Q-$Al_5Mg_8Cu_2Si_6$	E	21.1±0.9	32.7±0.8	-	24.3±0.6	21.9±0.4	-	-

Fig. 9. Representative FEG-SEM micrographs of the primary (**a, c**) and recycled (**b, d**) EN 45500 alloys in the T6 condition. The recycled alloy exhibits needle-like β-Al_5FeSi and π-$Al_8FeMg_3Si_6$ intermetallic compounds, while the primary alloy shows the presence of α-$Al_{15}(Fe,Mn,Cu)_3Si_2$ and minor π-$Al_8FeMg_3Si_6$. Both alloys contain Al_3Ti particles originating from grain refinement additions, with the recycled alloy also displaying Q-$Al_5Mg_8Cu_2Si_6$ intermetallic compounds.

elongation exhibit only minor variations, suggesting that the copper-based precipitation hardening in both alloys mitigates mechanical degradation during extended thermal exposure. This stability is particularly relevant for the recycled alloy, as it demonstrates that its higher Fe content does not compromise the long-term strength retention, further supporting its suitability for structural applications even under prolonged service conditions at high temperature.

3.6. Fractographic characterization

Fractographic analysis of the primary EN 45500 alloy after T6 heat treatment, shown in Fig. 12(a), reveals predominantly thin α-$Al_{15}(Fe,Mn,Cu)_3Si_2$ intermetallic compounds. In contrast, the recycled alloy (Fig. 12(b)) exhibits a high density of β-Al_5FeSi particles, indicating a greater susceptibility to fracture, consistent with the lower elongation values measured for this alloy. These plate-like intermetallics promote fracture surfaces with flat cleavage facets, indicative of localized brittle behaviour in regions surrounding these particles.

Beyond acting as stress concentrators, β-Al_5FeSi platelets also hinder interdendritic feeding during solidification, leading to the formation of shrinkage cavities that further reduce ductility. This combined effect is evident in the fracture behaviour shown in Fig. 13, which compares the

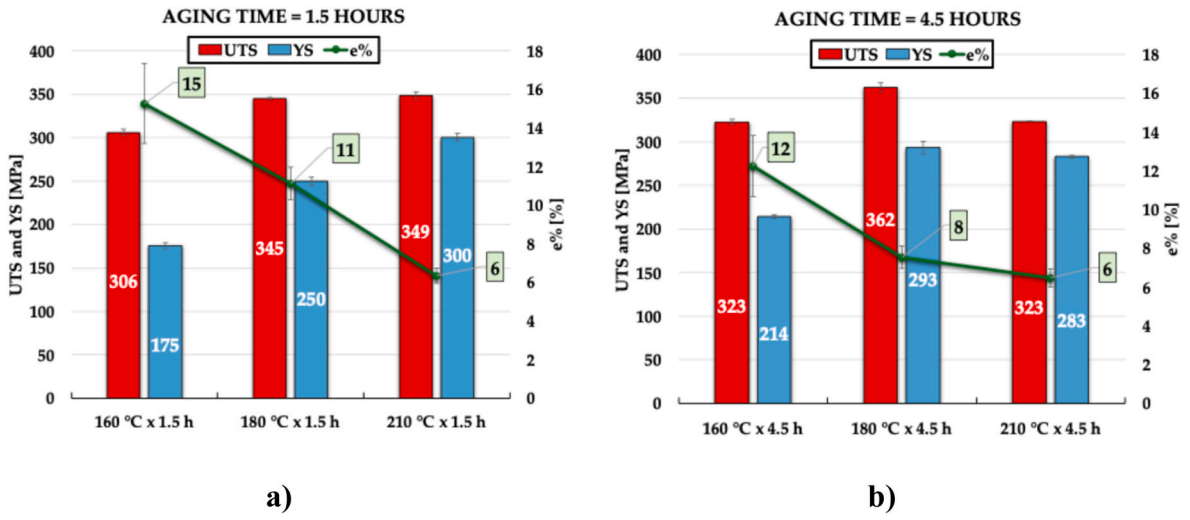

Fig. 10. Ultimate tensile strength (UTS), yield strength (YS), and elongation (e%) of the primary EN 45500 alloy after T6 aging at (**a**) 1.5 h and (**b**) 4.5 h at different temperatures (160 °C, 180 °C, 210 °C). Results highlight the trade-off between strength and ductility, with peak strength achieved at 180 °C for 4.5 h, while lower temperatures and times favour elongation.

Table 6
Ultimate tensile strength (UTS), yield strength (YS), elongation (e%), and toughness modulus (UT) of primary and recycled EN 45500 alloys under different T6 aging conditions. Percent variations for the recycled alloy are calculated relative to the peak-aged primary condition (180 °C for 4.5 h).

Alloy	Aging temperature [°C]	Aging time [h]	UTS [MPa]	YS [MPa]	e% [%]	UT [MJ/m^3]
EN 45500 Primary	180	4.5	362 ± 5	293 ± 7	7.5 ± 0.57	22.71 ± 5.13
EN 45500 Recycled	160	1.5	316 ± 9 (−12.7%)	187 ± 6 (−36.2%)	13.9 ± 1.5 (+85.3%)	38.42 ± 4.13 (+69.2%)
		4.5	339 ± 4 (−6.4%)	246 ± 2 (−16.0%)	9.9 ± 1.8 (+32%)	27.06 ± 6.11 (+19.2%)
		38	359 ± 3 (−0.8%)	304 ± 2 (+3.8%)	4.4 ± 0.4 (−41.3%)	11.14 ± 1.46 (−50.9%)

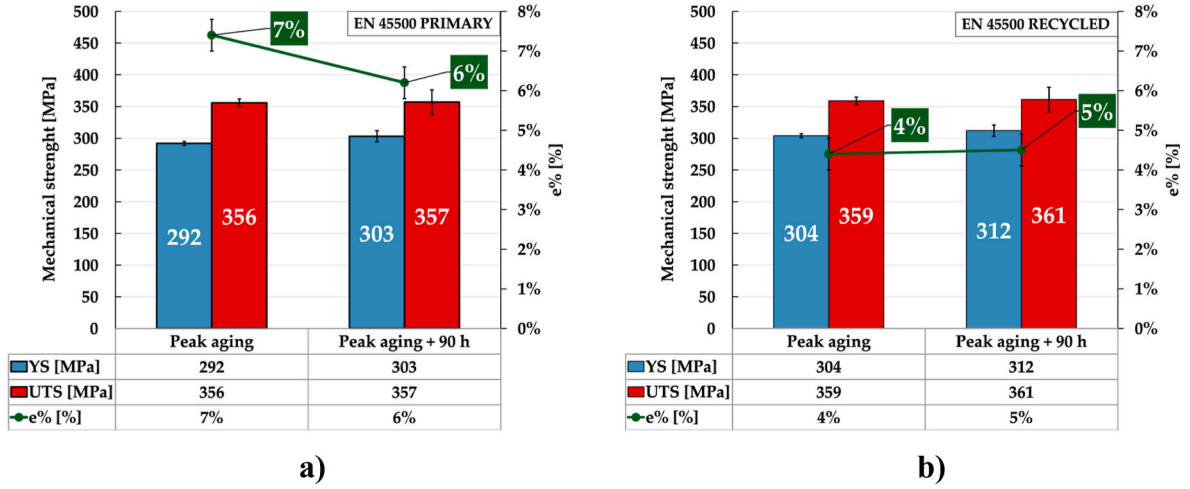

Fig. 11. Mechanical properties (YS, UTS, and e%) of primary (**a**) and recycled (**b**) EN 45500 alloys at peak aging (160 °C for 38 h) and after 90 h of overaging at 160 °C. Both alloys show negligible changes in tensile strength and elongation despite prolonged thermal exposure, indicating that their mechanical performance remains stable in the overaged condition.

fracture surfaces of the primary (Fig. 13(a)) and recycled (Fig. 13(b)) EN 45500 alloys aged at 160 °C for 4.5 h.

Although both alloys exhibit ductile fracture features characterized by deep dimples, the recycled alloy displays larger voids containing cracked silicon and intermetallic particles. The presence of shrinkage cavities further exacerbated this effect by acting as stress concentrators and promoting premature failure. This microstructural distinction accounts for the significantly lower elongation observed in the recycled alloy.

Compared with the T6 condition, the 160 °C for 128 h overaged specimens show a coarsening of the dimple structure in both alloys (Supplementary Fig. 2). However, in both alloys, fracture remains ductile, with uniformly distributed dimples. This observation is consistent with the mechanical characterization (Fig. 11), which highlighted a comparable overaged behaviour for the primary and recycled alloys, with only minor variations in strength and elongation compared to the peak aged condition.

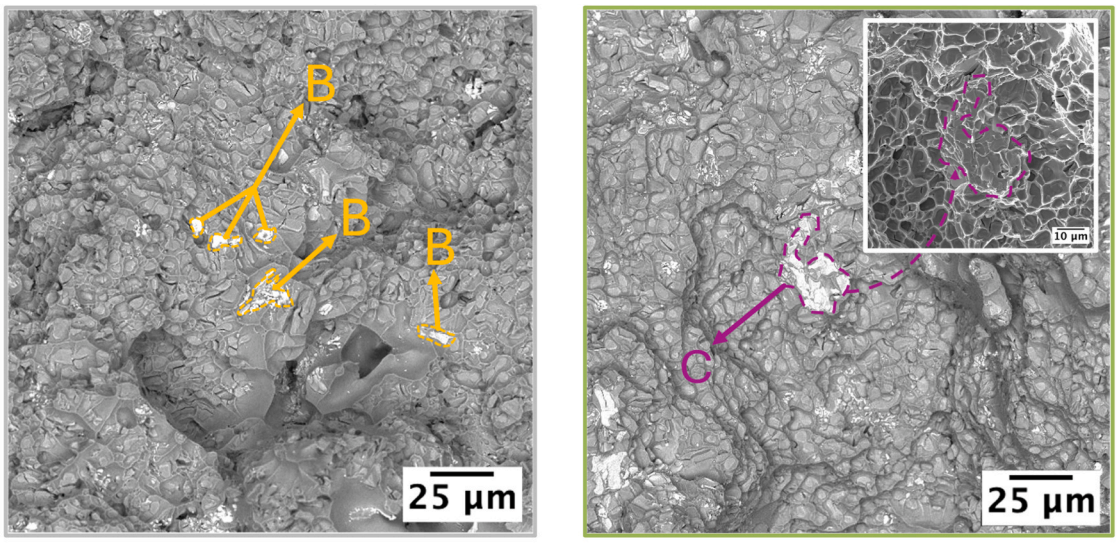

Identified Phase	Spot ID	Al (at.%)	Si (at.%)	Fe (at.%)	Mg (at.%)	Cu (at.%)	Mn (at.%)	Ti (at.%)
α-$Al_{15}(Fe,Mn,Cu)_3Si_2$	B	64.9±1.1	12.7±0.7	8.7±0.8	-	3.1±0.1	10.6±0.5	-
β-Al_5FeSi	C	68.5±0.8	16.5±0.8	15.0±0.4	-	-	-	-

Fig. 12. BSE FEG-SEM images of the fracture surfaces of (**a**) primary and (**b**) recycled EN 45500 alloys in the T6 condition. The primary alloy predominantly contains fine α-$Al_{15}(Fe,Mn,Cu)_3Si_2$ intermetallic compounds (highlighted with EDS composition), whereas the recycled alloy exhibits coarser β-Al_5FeSi platelets.

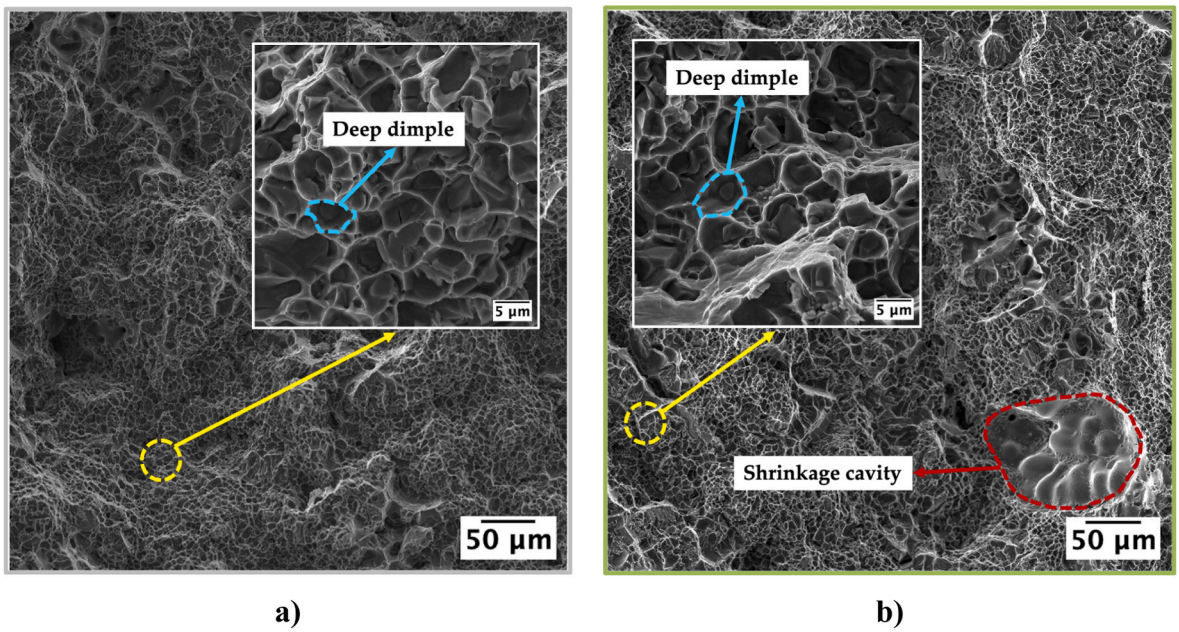

Fig. 13. SE FEG-SEM fracture surfaces of the primary (**a**) and recycled (**b**) EN 45500 in T6 condition. Both alloys exhibit ductile fracture features with deep dimples, while the recycled alloy additionally shows shrinkage cavities which explain the reduced elongation.

3.7. Environmental impact analysis

Fig. 14 illustrates the greenhouse gas emissions, expressed as $kgCO_{2eq}$/kgAl, associated with production and heat treatment EN 45500 alloy under three scenarios: primary aluminum produced using global average data, primary aluminum produced using European average data, and 100% recycled aluminum. While the substantially lower environmental impact of the recycled alloy mainly originates from the avoidance of the energy-intensive electrolytic process required for primary aluminum production, the results also highlight that the heat treatment stage represents a non-negligible contribution to the overall emissions. Although the remelting stage for the production of the analysed samples was excluded from the quantitative assessment, DSC analyses (Figs. 4–5) showed nearly identical melting behaviour and

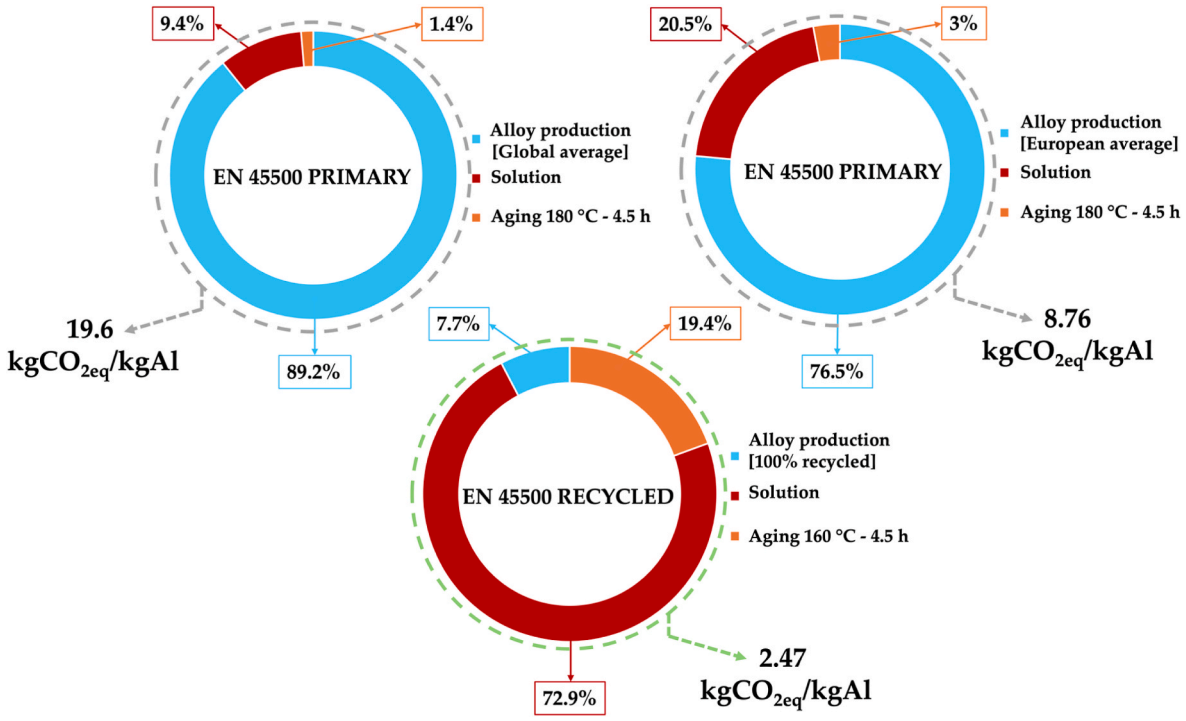

Fig. 14. Carbon footprint ($kgCO_{2eq}$/kgAl) of EN 45500 alloy production across three scenarios (primary – global average, primary – European average, and 100% recycled), calculated with contributions from alloy production, solution treatment, and aging.

transformation temperatures for the primary and recycled EN 45500 alloys, suggesting a thermodynamically comparable melting response. Therefore, the inclusion of the melting stage is not expected to alter the ranking between the different scenarios. Each chart displays the relative contributions of alloy production, solution treatment and optimized artificial aging (180 °C for 4.5 h for the primary alloy and 160 °C for 4.5 h for 100% recycled alloy).

The total carbon footprint decreases significantly across the three scenarios, from 19.6 $kgCO_{2eq}$/kgAl for primary aluminum (global average), to 8.76 $kgCO_{2eq}$/kgAl for primary aluminum (European average), and down to 2.47 $kgCO_{2eq}$/kgAl for the 100% recycled alloy. For primary alloys, the production stage is the dominant contributor, accounting for 89.2% of total emissions in the global average scenario and 76.5% in the European average scenario. In contrast, for the recycled alloy, heat treatment becomes the main hotspot, with solution treatment and aging together accounting for 92.3% of the total emissions, of which solution treatment alone representing 72.9%. These results highlight the importance of a detailed assessment of heat treatment stages when evaluating the environmental impact of recycled alloys. In this context, optimizing solution treatment parameters (as proposed by Merlin et al. (2025)), and reducing aging temperature and duration, as demonstrated in the present study, emerge as effective strategies to minimize emissions while retaining the required mechanical performance. Overall, the findings emphasize the critical role of recycled aluminum in reducing the carbon footprint of alloy production, as well as the need to target the alloy production stage for further decarbonization efforts.

4. Conclusions

This study investigated the mechanical and microstructural properties of a primary and a fully (100%) recycled EN 45500 alloy, both produced via gravity die casting and subjected to T6 heat treatment. The objective was to evaluate their performance, optimize thermal cycles, and assess their environmental impact, with particular attention to the influence of iron (0.15 wt% in the recycled alloy) on mechanical behaviour and resistance to overaging. The findings demonstrate that recycled EN 45500, when processed under specific aging conditions, can achieve mechanical properties comparable to those of the primary alloy while substantially reducing its carbon footprint. The key conclusions can be summarized as follows:

- Recycled EN 45500 achieves mechanical properties nearly identical to those of the peak aged primary alloy, when aged at 160 °C for 4.5 h, despite its higher iron content. This thermal cycle also requires significantly less energy than the standard 180 °C for 4.5 h aging treatment used for the primary alloy.
- Copper-driven thermal stability remains unaffected by moderate addition of iron ensuring long-term durability for structural components produced using recycled aluminum alloys
- The reduction in carbon footprint is substantial, with CO_{2eq} emissions as low as 2.47 $kgCO_{2eq}$/kgAl for the recycled alloy.
- Heat treatment accounts for 92.3% of the total emissions (excluding the casting phase from the assessment), making the optimization of solution treatment and aging parameters the most effective strategy for further reducing environmental impact.

CRediT authorship contribution statement

Cristian Cascioli: Writing – review & editing, Writing – original draft, Methodology, Investigation. **Linda Castagnini:** Writing – review & editing, Writing – original draft, Methodology, Investigation. **Alessandro Morri:** Validation, Supervision, Conceptualization. **Lorella Ceschini:** Validation, Supervision, Conceptualization.

Declaration of generative Ai and Ai-assisted technologies in the manuscript preparation process

No artificial intelligence tools were employed at any stage of the manuscript preparation process.

Funding

This study was financed by the European Union—NextGenerationEU (National Sustainable Mobility Center CN00000023, Italian Ministry of University and Research Decree n. 1033–17/06/2022, Spoke 11—Innovative Materials & Lightweighting). The opinions expressed are those of the authors only and should not be considered as representative of the European Union or the European Commission's official position. Neither the European Union nor the European Commission can be held responsible for them.

Declaration of competing interest

The authors declare that they have no known competing financial interests or personal relationships that could have appeared to influence the work reported in this paper.

Acknowledgements

The authors would like to thank Dott. Iuri Boromei for his support with the GD-OES analysis, Tommaso Merlini for his contribution during the development of his master's thesis, and Raffmetal S.p.A. for supplying the recycled aluminum ingots used in the present study. The authors have reviewed and edited the final manuscript and take full responsibility for the content of this publication.

Appendix A. Supplementary data

Supplementary data to this article can be found online at https://doi.org/10.1016/j.jclepro.2026.147718.

Data availability

Data will be made available on request.

References

BS EN 1706:2020, 2020. Aluminium and Aluminium Alloys. Castings. Chemical Composition and Mechanical Properties Table 1—Chemical Composition of Aluminium Castings. BSI Standards Publication, Bruxelles, Belgium.
BS EN ISO 6892-1:2019, 2019. Metallic Materials-Tensile Testing, Method of Test at Room Temperature. BSI Standards Publication, Bruxelles, Belgium.
Cagala, Mi, Bruska, M., Lichy, P., Beňo, J., Spirutova, e N., 2013. Influence of aluminium-alloy remelting on the structure and mechanical properties. Mater. Technol. 47, 239–243.
Callister, W.D., Rethwisch, e D.G., 2020. Materials Science and Engineering: an Introduction, 10st ed. Wiley.
Cascioli, C., Arcaleni, R., Morri, A., Ceschini, e L., 2025. Heat Treatment Analysis and Mechanical Characterization of a Recycled Gravity Die Cast EN 42000 Alloy. Metals 15 (7), 726. https://doi.org/10.3390/met15070726 fasc.
Ceschini, L., Boromei, I., Morri, A., Seifeddine, S., Svensson, e I.L., 2009. Microstructure, tensile and fatigue properties of the Al–10%Si–2%Cu alloy with different Fe and Mn content cast under controlled conditions. J. Mater. Process. Technol. 209 (15–16), 5669–5679. https://doi.org/10.1016/j.jmatprotec.2009.05.030 fasc.
Ceschini, L., Morri, A., Morri, A., Pivetti, e G., 2011. Predictive equations of the tensile properties based on alloy hardness and microstructure for an A356 gravity die cast cylinder head. Mater. Des. 32 (3), 1367–1375. https://doi.org/10.1016/j.matdes.2010.09.014 fasc.
Ceschini, L., Morri, A., Toschi, S., Seifeddine, e S., 2016. Room and high temperature fatigue behaviour of the A354 and C355 (Al–Si–Cu–Mg) alloys: role of microstructure and heat treatment. Mater. Sci. Eng., A 653, 129–138. https://doi.org/10.1016/j.msea.2015.12.015.
Chen, X., Brewer, T., Sever, C., Prabhu, E., Adimi, R., Engler-Pinto, e C., 2017. Cylinder Head Design Process to Improve High Cycle Fatigue Performance. presented at WCXTM 17: SAE World Congress Experience. https://doi.org/10.4271/2017-01-1074, 2017-01–1074.
Ciacci, L., Fishman, T., Elshkaki, A., Graedel, T.E., Vassura, I., Passarini, e F., 2020. Exploring future copper demand, recycling and associated greenhouse gas emissions in the EU-28. Glob. Environ. Change 63, 102093. https://doi.org/10.1016/j.gloenvcha.2020.102093 lug.
Di Sabatino, M., Arnberg, L., Rørvik, S., Prestmo, e A., 2005. The influence of oxide inclusions on the fluidity of Al–7wt.%Si alloy. Mater. Sci. Eng., A 413–414, 272–276. https://doi.org/10.1016/j.msea.2005.08.175.
Djurdjevic, M., Jiang, H., Sokolowski, e J., 2001. On-line prediction of aluminum–silicon eutectic modification level using thermal analysis. Mater. Char. 46 (1), 31–38. https://doi.org/10.1016/S1044-5803(00)00090-5 fasc.
Ducker, Ducker Public Summary, 2023. Aluminum Content in Passenger Vehicles. Europe.
E04 Committee, Guide for Preparation of Metallographic Specimens. doi: 10.1520/E0003-11R17.
E04 Committee, Practice for Microetching Metals and Alloys. doi: 10.1520/E0407-07R15E01.
E28 Committee, Test Method for Brinell Hardness of Metallic Materials. doi: 10.1520/E0010-18.
European Aluminium Brussels, 2020. A Strategy for Achieving Aluminium's Full Potential for Circular Economy by 2030. European Aluminium, Brussels, Belgium.
Harazeen, A., Lattanzi, L., Matsushita, T., Jarfors, e A.E. W., 2025. Enhanced iron impurity removal in low iron Al-Si alloys by Mn addition. HTHP 54 (2), 187–201. https://doi.org/10.32908/hthp.v54.1905 fasc.
Ibrahim, M., Elgallad, E., Valtierra, S., Doty, H., Samuel, e F., 2016. Metallurgical parameters controlling the eutectic silicon charateristics in Be-Treated al-si-mg alloys. Materials 9 (2), 78. https://doi.org/10.3390/ma9020078 fasc.
Koese, M., Parzer, M., Sprecher, B., Kleijn, e R., 2025. Self-sufficiency of the European union in critical raw materials for E-mobility. Resour. Conserv. Recycl. 212, 108009. https://doi.org/10.1016/j.resconrec.2024.108009 gen.
Li, L., Li, D., Feng, J., Zhang, Y., Kang, e Y., 2020. Effect of Cooling Rates on the Microstructure and Mechanical Property of La Modified Al7SiMg Alloys Processed by Gravity Die Casting and Semi-Solid Die Casting. Metals 10 (4), 549. https://doi.org/10.3390/met10040549 fasc.
Li, S., et al., 2023. Development and applications of aluminum alloys for aerospace industry. J. Mater. Res. Technol. 27, 944–983. https://doi.org/10.1016/j.jmrt.2023.09.274.
Li, X., et al., 2025. Effect of Cu and Zn on microstructure and mechanical properties of Al-Mg-Si cast alloy. J. Alloys Compd. 1036, 181688. https://doi.org/10.1016/j.jallcom.2025.181688 lug.
Merlin, M., Antonioli, L., Bin, F., Morales, C., Soffritti, e C., 2025. On the optimization of T6 heat treatment parameters of a secondary al-si-cu-mg foundry aluminum alloy: a microstructural and mechanical characterization. Metals 15 (7), 742. https://doi.org/10.3390/met15070742 fasc.
Nunes, H., Emadinia, O., Soares, R., Vieira, M.F., Reis, e A., 2023. Adding value to secondary aluminum casting alloys: a review on trends and achievements. Materials 16 (3), 895. https://doi.org/10.3390/ma16030895 fasc.
Perrin, T., Després, A., Heugue, P., Deschamps, A., De Geuser, e F., 2025. High-throughput characterisation of the long-term ageing of an A357+1wt%Cu cast aluminium alloy using temperature gradient. Materialia 39, 102378. https://doi.org/10.1016/j.mtla.2025.102378.
Puncreobutr, C., Lee, P.D., Kareh, K.M., Connolley, T., Fife, J.L., Phillion, e A.B., 2014. Influence of Fe-rich intermetallics on solidification defects in Al–Si–Cu alloys. Acta Mater. 68, 42–51. https://doi.org/10.1016/j.actamat.2014.01.007.
Raabe, D., et al., 2022. Making sustainable aluminum by recycling scrap: the science of "dirty" alloys. Prog. Mater. Sci. 128, 100947. https://doi.org/10.1016/j.pmatsci.2022.100947 lug.
Raffmetal, S.p.A., 2023. Environmental product declaration (EPD): aluminium alloys from recycling S-P-06061. EPD Programme Operator: International EPD® System. ISO 14025, third-party verified.
Raffmetal, S.p.A., 2025. SILVAL Primary Aluminium Alloys from Recycling [Technical brochure].
Ravindran, E. Vandersluis e C., 2017. Comparison of measurement methods for secondary dendrite arm spacing. Metallogr. Microstruct. Anal. 6 (1), 89–94. https://doi.org/10.1007/s13632-016-0331-8 fasc.
Rolseth, A., Carlson, M., Ghassemali, E., Pérez Caro, L., Jarfors, e A.E. W., 2024. Impact of functional integration and electrification on aluminium scrap in the automotive sector: a review. Resour. Conserv. Recycl. 205, 107532. https://doi.org/10.1016/j.resconrec.2024.107532.
Samuel, A.M., 2012. A review on the heat treatment of Al-Si-Cu/Mg casting alloys. In: Heat Treatment - Conventional and Novel Applications. F. Czerwinski, A c. di, InTech. https://doi.org/10.5772/50282.
Stanić, D., Zovko Brodarac, Z., Li, e L., 2020. Influence of copper addition in AlSi7MgCu alloy on microstructure development and tensile strength improvement. Metals 10 (12), 1623. https://doi.org/10.3390/met10121623 fasc.
Taylor, J.A., 2004. The Effect of Iron in Al-Si Casting Alloys. Australian Foundry Institute (AFI), Adelaide, Australia, pp. 148–157.
Toschi, S., 2018. Optimization of A354 al-si-cu-mg alloy heat treatment: effect on microstructure, hardness, and tensile properties of peak aged and overaged alloy. Metals 8 (11), 961. https://doi.org/10.3390/met8110961 fasc.
Wang, Q., Hao, Q., Yu, e W., 2019. Effect of strontium modification on porosity formation in A356 alloy. Inter Metalcast 13 (4), 944–952. https://doi.org/10.1007/s40962-018-00300-1 fasc.
Zyska, A., 2021. Comparison of the porosity of aluminum alloys castings produced by squeeze casting. Manufacturing Technology 21 (5), 725–734. https://doi.org/10.21062/mft.2021.074 fasc.
ISPRA, 2025. CO_2 Emissions in the National and Regional Electricity Sector. Report 413/2025, Rome, Italy.